Electric field and electron density measurements of nanosecond repetitively pulsed microplasmas in atmospheric air

T. Orriere, N. Benard, E. Moreau and D. Z. Pai

Institut PPRIME (CNRS UPR 3346, Université de Poitiers, ISAE-ENSMA).
SP2MI – Teleport2 Bd Marie & Pierre Curie BP 30179, 86962 Futuroscope, France

Abstract: This paper presents results on nanosecond repetitively pulsed microplasmas are generated in atmospheric air in a pin-to-pin configuration. This regime is mainly studied by optical diagnostics such as ICCD visualisation and optical emission spectroscopy. Both techniques show the evolution of a streamer-less breakdown. The discharge dynamics and the chemistry are discussed for gap distances of 1 mm and 200 µm.

Keywords: microplasma, optical emission spectroscopy, nanosecond repetitively pulsed discharges.

1. Introduction

Non-thermal plasmas in atmospheric air are useful for many fields such as biomedicine, aerodynamic flow control [1], materials processing, combustion, and nanomaterials synthesis [2]. Because of air properties such as high pressure or complex plasma chemistry, the selection of useful reactions and power management for applications are hard challenges. That is why it is necessary to control the main characteristics of discharges in air using methods such as adding a dielectric barrier. But this type of discharge has low electron density and chemical reactivity. Another type of discharge which permits to reach high electron densities is the spark or arc discharge but the presence of oxygen leads to significant heating, which could be a problem for equipment safety or the treatment of thermally sensitive surfaces such as plastics, food or biological tissue.

These disadvantages can be overcome by using nanosecond repetitively pulsed (NRP) discharges [3]. The aim of this study is to confine NRP discharges in atmospheric air to 200 µm (i. e. NRP microplasmas) in a pin-to-pin configuration and compare selected plasma properties to NRP spark discharges at 1 mm. We will present measurements of electric field electron number density. Also, ICCD images of the discharge are presented with electrical diagnostics to describe the dynamics of the discharge.

2. Experimental setup

As shown on figure 1, NRP microplasmas and mm-scale sparks were generated by applying pulses up to 6 kV between two tungsten electrodes separated by a gap distance of 200 µm or 1 mm in air at room conditions. A high voltage nanosecond pulse generator (FID Technology FPG 40-30 NK) was used, and impedance matching was achieved with two resistances 200 Ω and 100 Ω in value. The radius of curvature of the electrodes was 280 µm. The voltage across the gap was measured by a passive probe (Lecroy PPE 6 kV, bandwidth 400 MHz), and the discharge current was measured by a current transformer (Bergoz CT-D5.0, bandwidth 400 MHz). These signals were recorded with oscilloscope (WaveRunner 204 MXI, 2 GHz bandwidth, 5 GS.s^{-1}). The delay between the current and the voltage is determined by contacting the two pins to determine the stray inductance L_{cable} = 0.2µH between the ground and the point where the voltage is measured (~230 mm of cable length away from the discharge gap). The voltage across the gap (V_{plasma}) was calculated by correcting the measured voltage V_{probe} by using equation 1. Due to the low capacitance between electrodes (2.4 pF), the conduction current I_{plasma} is approximated as the current measured by the probe I_{probe}.

$$V_{plasma}(t) = V_{probe}(t) - L\frac{dI_{probe}(t)}{dt} \quad (1)$$

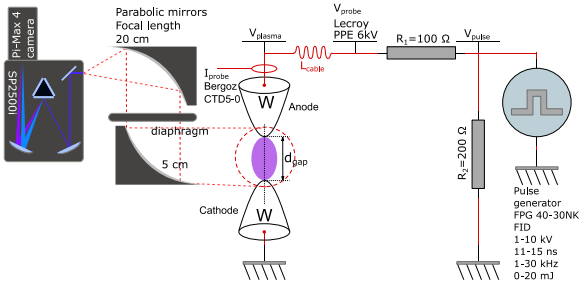

Fig. 1. Experimental setup for discharge generation and diagnostics

All measurements were synchronized by a trigger source (Stanford Research systems DG645). Optical emission spectroscopy (OES) was performed with a spectrometer (Acton SP2500i) equipped with an ICCD camera (Princeton instrument PI-MAX 4). ICCD images are recorded trough the spectrometer with the grating centred at 0 nm. The optical path was formed by two off-

axis parabolic mirrors with focal lengths of 5 and 20 cm. The total magnification was m = 4.4, and a diaphragm was placed between the mirrors to increase the depth of field, which increased spatial resolution and the intensity of the signal.

3. Experimental method

Even if tungsten is an interesting spark resistant material [2], erosion due to the high repetition frequency has to be taken into account. First of all, the gap distance and electrode radius of curvature increase during the experiment.

Table 1. OES acquisition parameters

Central Wavelength (nm)	Grating ($gr.mm^{-1}$)	Information	Time steps / accumulations
394	1800	E/N; N_2, N_2^+	38 / 30 × 5000
377	2400	N_2	9 / 30 × 5000
656	600	H_α	14 / 30 × 5000

To minimize the effect of changing electrode conditions, we need to optimize the amount of information acquired per discharge event. This was achieved by properly choosing the spectrometer settings for acquisitions, as shown on Table 1.

The electric field is estimated by using the intensity ratio $I_{391.4\ nm}/I_{394\ nm}$ between the second positive system (SPS) of the N_2 ($C^3\prod_u \rightarrow B^3\prod_g$) 2-5 band ($I_{394\ nm}$) and the first negative system (FNS) of the N_2^+ ($B^2\sum_g^+ \rightarrow X^2\sum_g^+$) 0-0 band ($I_{391.4\ nm}$). We consider that the $N_2(C)$ and N_2^+ (B) are populated from $N_2(X)$ by electron-impact excitation and that the decay lifetime of these species is determined by gas phase quenching and radiation. Based on the steady-state approximation of this calculation, which has been used in most studies similar to ours, empirical relationships of the electric field to the ratios $I_{391.4\ nm}/I_{337.1\ nm}$ and $I_{391.4\ nm}/I_{394\ nm}$ have been derived in room conditions between 150-5000 Td [4] where $I_{337.1}$ is the intensity of the the N_2 ($C^3\prod_u \rightarrow B^3\prod_g$) 0-0 band. An exhaustive set of reaction constants for the quenching is proposed in [5], but we chose to use sets measured with similar experimental conditions in [6,7]. However, we determined an error bar based on reaction constants from [5].

Table 2. Quenching rate constants used in this work

State	i	Radiative lifetime	Deactivation rate constants	
Symbol	-	τ^i_0	k^1_{qN2}	k^1_{qO2}
Unit	-	ns	$10^{-10}\ cm^3.s^{-1}$	
N_2 ($C^3\prod_u$, v = 2) [6]	C	39 ± 4	0.46 ± 0.06	3.7 ± 0.5
N_2^+ ($B^2\sum_g^+$, v = 0) [7]	B	62 ± 6	2.1 ± 0.2	5.1 ± 0.5

The electron density can be deduced by using the full width at half maximum (FWHM) or the full width at half area (FWHA) of the Stark broadening of the H_α line. Several processes of different nature can be involved in the broadening of a line but Stark broadening is dominant in our conditions. First, the transfer function of the optical path is corrected. Second, datasets are fitted with three Voigt profiles f(λ), corresponding to the H_α line and the two N^+ lines ($^1P° \rightarrow {}^1P$) 648.2 nm and ($^1D \rightarrow {}^1F°$) 661.1 nm, as well as a linear background. The fit is performed with the Lmfit package for Python [8]. The instrumental function is determined with a Voigt fitting and σ_i = 63.13 pm and γ_i = 32.82 pm, where σ_i and γ_i are the widths of the Gaussian and Lorentzian shape contributions. The FWHA is computed by integrating the Lorentzian part of the fitted profile of the H_α line. The electron density deduced from the FWHA is thus [9]. Another formula from [10] that is fitted using data from [9] uses the full width at half maximum (FWHM) to calculate electron number density.

4. Results and discussion

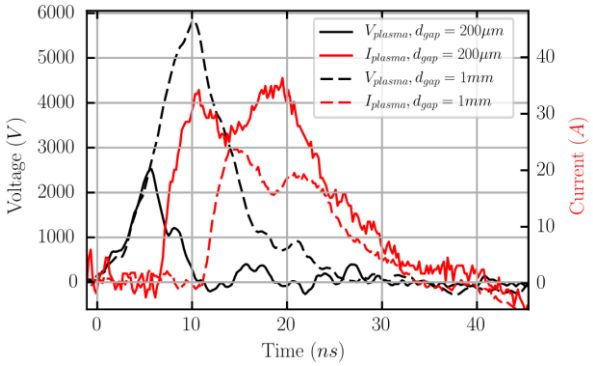

Fig. 2. Single shots of discharge current and voltage for two different gap distances. The energy was 100.2 µJ for d_{gap} = 200 µm and 403.9 µJ for d_{gap} = 1 mm.

Figure 2 shows typical current-voltage waveforms of NRP microplasmas in air compared with a 1-mm NRP spark. For both cases, the power supply was set to reach a maximum voltage of 6 kV between the electrodes when there is no breakdown. This value also represents the maximum voltage measureable by our voltage probe. The discharge jitter relative to the position of the maximum voltage around 0.4 ns. At d_{gap} = 1mm, the energy was 400.89 ± 31.92 µJ. By assuming that the gas density N changes due to temperature rather than changes in the chemical composition of the air between pulses, the reduced electric field can be calculated as: E/N (Td) = $10^{21} \times V_{plasma}$ (V) × k_b ($m^2.kg.s^{-2}.K^{-1}$) × T_{gas}(K) / (d_{gap}(m) × P_{atm} (Pa)) with the k_b Boltzmann constant, T_{gas} is the gas temperature which has been measured with the SPS of N_2 at the beginning of the pulse, and P_{atm} is atmospheric pressure. With d_{gap} = 1 mm, the voltage reached 5.86 kV and the gas temperature has been determined to be 400 K. Therefore the maximum electric field during the pulse

reaches 320 Td. This value is consistent with previously reported electric fields of 300 Td for similar discharges in preheated air at 1500 K [11]. With d_{gap} = 200 µm the energy was 110.98 ± 12 µJ. In this condition T_{gas} = 370 K and the voltage reached 2.33 kV which corresponds to a maximum electric field of 590 Td. Thus the applied electric field for the micrometer case is much higher than for the millimeter case. The energy per unit gap distance is ~39 % higher with the microplasma case, which indicates a discharge with a higher energy density.

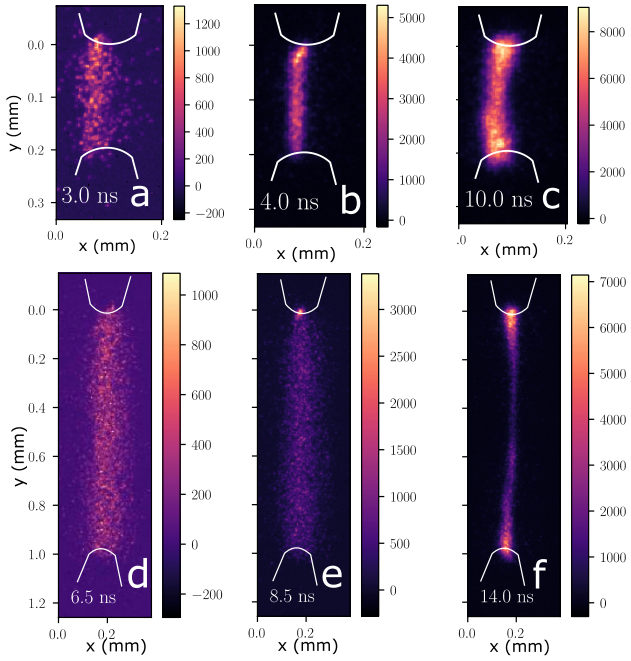

Fig. 3. Single shots images of NRP discharges for d_{gap} = 200 µm and d_{gap} = 1 mm (bottom). The gain was kept constant, and the exposure time was 3 ns. The axes are in units of mm, and the colorbar shows the intensity of the signal. The cathode is placed at y = 0 mm.

Figure 3 shows single shot images of the discharge for d_{gap} = 200 µm and 1 mm. The gate was open during 3 ns, so there is an overlap between images 3a and 3b and the jitter of the discharge was < 0.5 ns with d_{gap} = 200 µm and 1.4 ns with d_{gap} = 1 mm. Due to the high reproducibility of NRP discharges, we assume an image sequence is representative of a single discharge. By comparing with figure 2, we see that images a), b) d) and e) occur during the rise time of applied voltage, and images c) and f) occur during the fall time. Both cases show the same discharge evolution at the beginning with diffuse emission over the entire gap. On images b) and e), there is strong emission near the cathode just before the rise of the current. Just afterwards, the discharge channel is strongly constricted into a single filament. For both gap distances, the images do not indicate ionization wave propagation or streamers but rather a Townsend discharge, although the temporal resolution maybe insufficient. Another study in pure N_2 at atmospheric pressure without preheating but at lower PRF (1 kHz) shows a different comportment with a discharge moving from the anode to the cathode [10]. The same uniform breakdown has already been reported with a similar discharge in preheated air, with a larger gap and higher PRF [12]. In that study, the authors showed that streamer-less breakdown can occur for NRP sparks and listed conditions for which this can occur. Since high pre-ionization is necessary, particular attention has to be paid to the PRF and the electronegativity of the gas which can influence the pre-ionization.

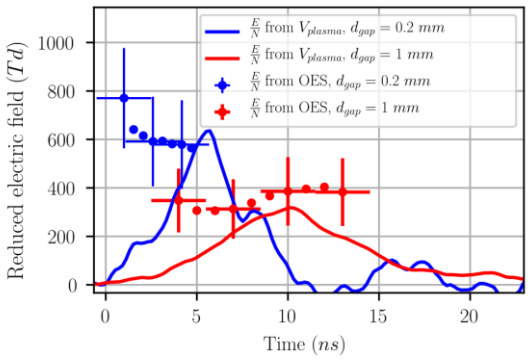

Fig. 4. Average electric field in the gap deduced from voltage measurements and OES.

We used the intensity ratio of FNS N_2^+ and the SPS of N_2 to deduce the electric field. The average electric field in the gap has been obtained by integrating the spatially resolved electric field along the discharge axis by using a trapezoidal rule and then dividing by the gap distance. On Figure 4, we compare values obtained by OES and by electrical measurements. Error bars for the OES measurement reflect the uncertainty in the appropriate quenching rates and the dissociation degree. However, the measurement is most valid at the beginning of the discharge because we expect the dissociation degree to be weak at this time. At later times, OES of the discharge shows the emission of O, O^+, N and N^+ lines, and we would expect strong dissociation and thus poor validity of OES measurements of the electric field. Yet paradoxically, the largest disagreement between the two measurement techniques occurs at the beginning for both cases. This difference between the two curves could have several explanations: the zone where the electric field is very high is near the cathode because of the strong emission of N_2^+ at this location. If the depth of field is thinner than this zone, then we overestimate the length of this region (~40 µm), and this could lead to an error upon integration. Second, the temperature measurement by optical emission spectroscopy is not discussed in detail here, but an underestimation by 150 K of the temperature could also lead to an underestimation by about 120 Td in the electric field calculated using the voltage curves. Finally the impact of the time integration of 3 ns of the optical system may also introduce error.

As described before, the electron density is measured by the Stark broadening of the H_α line. The measured electron density is on the order of 2×10^{18} cm^{-3} 30 ns after breakdown. We were not able to measure it at earlier time, because of the overlapping spectra of ions. We can first notice that the electron density given by FWHM and FWHA differ by less than a factor of two. The decay time can be determined and seems to follow two linear decays in the log scale between the intervals 30-100 ns and 100 - 300 ns. Both methods give a similar decay rate $k_1 = 1/\tau_1 = (27.4 \pm 1.2) \times 10^6\ s^{-1}$ and $k_2 = 1/\tau_2 = (12.1 \pm 0.2) \times 10^6\ s^{-1}$.

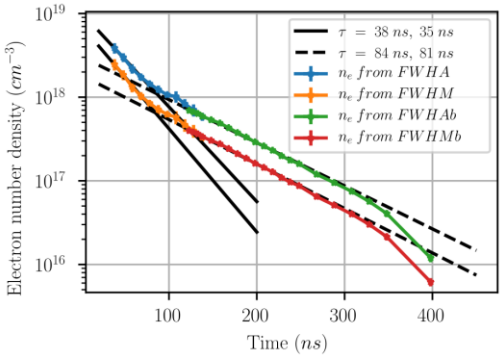

Fig. 5. Measured electron density by Stark broadening of the H_α line for d_{gap} = 200 µm. Due to weak emission, data points marked "b" have been recorded with more accumulations than for the measurements discussed in table 1.

5. Conclusion

NRP discharges in the microplasma regime have been studied and compared to mm-scale sparks. Initially, the discharge does not show streamer propagation but rather uniform Townsend ionization. Two phases at the beginning of the discharge have been identified. We showed first a diffuse emission which can be due to a Townsend phase. The second phase is characterized by the constriction of the filament and the strong emission of ions lines. The electric field has been measured by OES and voltage measurements but shows a disagreement at the beginning of the pulse where we expected both methods to be valid. The electron density reaches around 10^{18} cm^{-3}. The chemistry just after the Townsend phase and during the afterglow will be discussed further later. Possible reactions for the electron decay during the first 100 ns of the discharge will also be discussed.

6. Acknowledgements

This work has been supported by the French Government program "Investissements d'Avenir" (LABEX INTERACTIFS, reference ANR-11-LABX-0017-01), the Poitou-Charentes region (CPER program), the European Union (FEDER/FSE/FEADER programs), and the Agence Nationale de la Recherche programs INOPLAS (ANR-13-ASTR-0015-01) and PLASMAFACE (ANR-15-CE06-0007-01). T. Orrière has been supported by a PhD fellowship from the Ministère de l'Education Nationale, de l'Enseignement Supérieur et de la Recherche.

7. References

[1] K. D. Bayoda, N. Benard, and E. Moreau, J. Appl. Phys. **118**, 063301 (2015).

[2] N. S. Tabrizi, M. Ullmann, V. A. Vons, A. Schmidt-Ott, and U. Lafont, J. Nanoparticle Res. 11 2 (2008).

[3] D. Packan, Ph.D. thesis, Stanford University, 2003.

[4] P. Paris, M. Aints, F. Valk, T. Plank, A. Haljaste, K. V. Kozlov, and H.-E. Wagner, J. Phys. Appl. Phys. **38**, 3894 (2005).

[5] G. Dilecce, P. F. Ambrico, and S. D. Benedictis, J. Phys. Appl. Phys. **43**, 195201 (2010).

[6] S. V. Pancheshnyi, S. M. Starikovskaia, and A. Y. Starikovskii, Chem. Phys. **262**, 349 (2000).

[7] S. V. Pancheshnyi, S. M. Starikovskaia, and A. Y. Starikovskii, Chem. Phys. Lett. **294**, 523 (1998).

[8] M. Newville, T. Stensitzki, D. B. Allen, and A. Ingargiola, https://zenodo.org/record/11813 (2014).

[9] M. A. Gigosos, M. Á. González, and V. Cardeñoso, Spectrochim. Acta Part B At. Spectrosc. **58**, 1489 (2003).

[10] R. M. van der Horst, T. Verreycken, E. M. van Veldhuizen, and P. J. Bruggeman, J. Phys. Appl. Phys. **45**, 345201 (2012).

[11] D. L. Rusterholtz, D. A. Lacoste, G. D. Stancu, D. Z. Pai, and C. O. Laux, J. Phys. Appl. Phys. **46**, 464010 (2013).

[12] D. Z. Pai, D. A. Lacoste, and C. O. Laux, Plasma Sources Sci. Technol. **19**, 065015 (2010).